Lab on a Chip

PAPER

View Article Online
View Journal | View Issue

Cite this: *Lab Chip*, 2026, **26**, 375

Advancing liquid biopsy: whispering gallery mode laser detection of the HER2 cancer biomarker on extracellular vesicles

Sentayehu Fetene Wondimu,†[ab] Richa Khanduri,†[c] John Atanga,[c] Marc Hippler,[abd] Andreas Hofmann,[e] Christoph Hussal,[f] Daria Kohler,[ab] Sarah Krämmer,[d] Uwe Bog,[a] Tobias Wienhold,[a] Meike Koenig,[f] Sebastian Köber,[ab] Timo Mappes,‡[a] Joerg Lahann,[fk] Heinz Kalt,[d] Wolfgang Freude,[ab] Johnathan Sleeman,[g] Athanasia Warnecke,[h] Thalia Erbes,[ij] Ingolf Juhasz-Böss,[ij] Christian Koos[ab] and Irina Nazarenko *[c]

The search for new technologies to reliably detect biomarkers in body fluids has become critical for the integration of liquid biopsy into routine diagnostics. Among the most important applications is the need for effective monitoring of therapy response and early detection of emerging resistance. However, the availability of robust and quantitative tools for measuring biomarkers in body fluids remains limited. HER2, the epidermal growth factor receptor-2, is of significant importance as a predictive biomarker and therapeutic target, not only in breast cancer, but also in colorectal, gastric, prostate and other malignancies. Tumors that express HER2 are susceptible to HER2-targeted therapies, which include inhibitory antibodies such as trastuzumab and pertuzumab, as well as small inhibitor molecules such as lapatinib and tucatinib. Despite the success of these treatments, more than 20% of patients develop resistance. The most common mechanisms of resistance are either cleavage of HER2 leading to the formation of an intracellular, constitutively active, ligand-independent p95HER2 protein and its extracellular p105HER2 counterpart, or the formation of HER2/HER3 heterodimers. Current clinical diagnostics are primarily limited to detecting HER2 in tissue biopsies, which cannot be routinely performed during treatment due to the invasive nature and high patient burden of tissue sampling. Additionally, while soluble p95HER2 protein can be measured in patient serum using conventional ELISA, this method lacks robust prognostic value. The detection of full-length HER2 in the form of homo- and heterodimers is still lacking and could be a key element in establishing liquid biopsy-based HER2 therapy monitoring. In this manuscript, we propose a novel approach using whispering gallery mode (WGM) lasers as a reliable method to specifically detect full-length HER2 proteins associated with extracellular vesicles (EVs) released into the circulation. We have successfully established a detection limit of 10^7 vesicles per mL, approximately equivalent to 10 μL of human plasma or serum. Moreover, our detection technology can discriminate between soluble HER2 and membrane-bound HER2, enabling precise identification of the latter. This

Received 14th March 2025,
Accepted 4th September 2025

DOI: 10.1039/d5lc00269a

rsc.li/loc

[a] *Institute of Microstructure Technology (IMT), Karlsruhe Institute of Technology (KIT), Hermann-von-Helmholtz-Platz 1, 76344 Eggenstein-Leopoldshafen, Germany*
[b] *Institute of Photonics and Quantum Electronics (IPQ), KIT, Engesserstr. 5, 76131 Karlsruhe, Germany*
[c] *Faculty of Medicine, Institute of Infection Prevention and Control, University Medical Center Freiburg, Breisacher Strasse 115 B, 79106 Freiburg, Germany. E-mail: irina.nazarenko@uniklinik-freiburg.de*
[d] *Institute of Applied Physics (APH), KIT, Wolfgang-Gaede-Str. 1, 76131 Karlsruhe, Germany*
[e] *Institute of Applied Computer Science (IAI), KIT, Hermann-von-Helmholtz-Platz 1, 76344 Eggenstein-Leopoldshafen, Germany*
[f] *Institute of Functional Interfaces (IFG), KIT, Hermann-von-Helmholtz-Platz 1, 76344 Eggenstein-Leopoldshafen, Germany*
[g] *Institute of Toxicology and Genetics, Karlsruhe Institute of Technology (KIT), Hermann-von-Helmholtz-Platz 1, 76344 Eggenstein-Leopoldshafen, Germany*
[h] *Department of Otorhinolaryngology, Hannover Medical School, Carl-Neuberg-Str. 1, 30625 Hannover, Germany*
[i] *Department of Obstetrics and Gynecology, Medical Center - University of Freiburg, Freiburg, Germany*
[j] *Faculty of Medicine, 6, 79106 Freiburg, Germany*
[k] *Biointerfaces Institute, University of Michigan, Ann Arbor, Michigan 48109, USA*
† First two authors equally participated in this work.
‡ Current address: Deutsches Optisches Museum, Carl-Zeiss-Platz 12, 07743 Jena, Germany. Physikalisch-Astronomische Fakultät, Friedrich-Schiller-Universität Jena, Max-Wien-Platz 1, 07743 Jena, Germany.

advancement opens up the possibility of introducing HER2 detection as a highly accurate and quantitative liquid biopsy method for detecting HER2 in blood, in full-length forms, offering new avenues for non-invasive diagnostics, patients monitoring, and early prediction of therapy.

1. Introduction

Extracellular vesicles (EVs) have recently emerged as a crucial means of cellular communication. These vesicles are naturally present in body fluids like blood, saliva, urine, breast milk, and others.[1–4] They serve as messengers transporting information in the form of lipids, proteins, RNA, and potentially DNA between the cells, or as regulators of signal transduction cascades, activating cell surface receptors by the interaction with the cells.[5,6] EVs have a significant impact on both local cellular processes and systemic events, altering properties of recipient cells. Initially considered as mere membrane debris with no biological relevance, EVs are recognized to play essential roles in physiological and pathological processes including development, cancer, immunity and neurodegenerative diseases.[7–11] They are composed of heterogeneous populations of vesicles of different origins and sizes. Some of them are continuously released as an entire part of autocrine and paracrine regulation of homeostasis, as *e.g.* exosomes, which are formed by the intraluminal budding of endosomal membranes.[5] Other types of vesicles are shed in response to exogenous stimuli, such as alterations in pH, hypoxia, irradiation, cellular injury, and physiological stressors.[12,13] Additionally, when the cells undergo apoptosis, due to the actomyosin contractions and cytoskeleton destruction, apoptotic blebs, also considered as another EV type, are released.[14] Regardless of their origin, EV content reflects the molecular composition of donor cells, making them a valuable source of potential biomarkers.[15,16]

Depending on the isolation method, different EV populations can be enriched. However, none of the isolation methods allows absolute separation of a particular EV population from others.[2] Speaking of blood-derived EVs, their isolation is even more complex because blood is enriched in a number of non-EV components, including proteins and lipoproteins; furthermore, the pre-analytical routine of blood collection can greatly affect the quality of EV isolates.[17,18] Therefore, technologies enabling sensitive and robust detection of EV-associated biomarkers, independent of sample purity, are highly desirable for advancing EV-based liquid biopsy in diagnostics and treatment monitoring.

HER2 overexpression characterizes 20–30% of breast cancer cases, correlating with adverse prognostic outcomes because of increased tumor cell proliferation, metastasis and tumor recurrence.[19,20] Current guidelines from the National Comprehensive Cancer Network recommend testing for HER2 expression in recurrent, unresectable, or metastatic salivary tumors as part of a biomarker panel, indicating the emerging role of HER2 expression as a biomarker and treatment target for malignancies of the head and neck.[21] At the same time, HER2 expression serves as an utmost valuable biomarker for the susceptibility for HER2-targeted therapy.[22] Presently, clinical diagnostic methodologies for HER2 evaluation are predominantly confined to the analysis of tissue biopsies or the assessment of cleaved HER2 extracellular domains (p105HER2) within serum samples, *e.g.* by using conventional ELISA. However, the latter approach does not discriminate between cleaved and membrane-bound HER2, limiting substantially its usefulness for the monitoring of therapy response and early detection of therapy resistance. Considering that HER2 can be released not only in its cleaved form as a soluble protein, but also as an EV-associated full-length protein,[23–27] we aimed to develop a new method that would allow selective detection of membrane-bound HER2 in a blood sample. To this end, we took advantage of the ability of WGM lasers to produce distinct, well-defined emission peaks.[28,29] When interacting with biological analytes, these peaks shift depending on the concentration of the analyte bound to the laser surface.[28,30] WGM lasers have been successfully used to detect a wide range of biomolecules, including oligonucleotides, nanoscale particles, cancer biomarkers, and viruses.[31,32] In our previous work, we demonstrated the applicability of WGM lasers in laboratory diagnostics by fabricating them at low cost and integrating them seamlessly into microfluidic systems, enabling automated lab-on-chip platforms.[29,33] In the current manuscript, we demonstrate the application of WGM lasers as the core component of a lab-on-chip platform for the detection of EVs and EV-bound HER2.

2. Results & discussion

2.1 The principle of EV-bound HER2 detection using a WGM laser chip

The physical detection principle of whispering gallery mode (WGM) lasers is based on shifts in the emission spectrum resulting from the attachment of particles or biomolecules to the resonant laser modes at the sensor surface. For the detection of extracellular vesicles (EVs), a chip containing 16 WGM lasers was fabricated as previously described[30] (Fig. 1A and B). We harness the fundamental working mechanism of WGM lasers by introducing molecular specificity through selective surface functionalization, using a chemistry approach detailed in our earlier work.[29] Precisely, in this study, the laser surfaces were functionalized with antibodies targeting specific membrane proteins on EVs (Fig. 1C), as described in the Methods section. For example, to enable detection of HER2-positive EVs, the laser surfaces were functionalized with HER2-specific antibodies, allowing selective immobilization of HER2-expressing EVs. Their

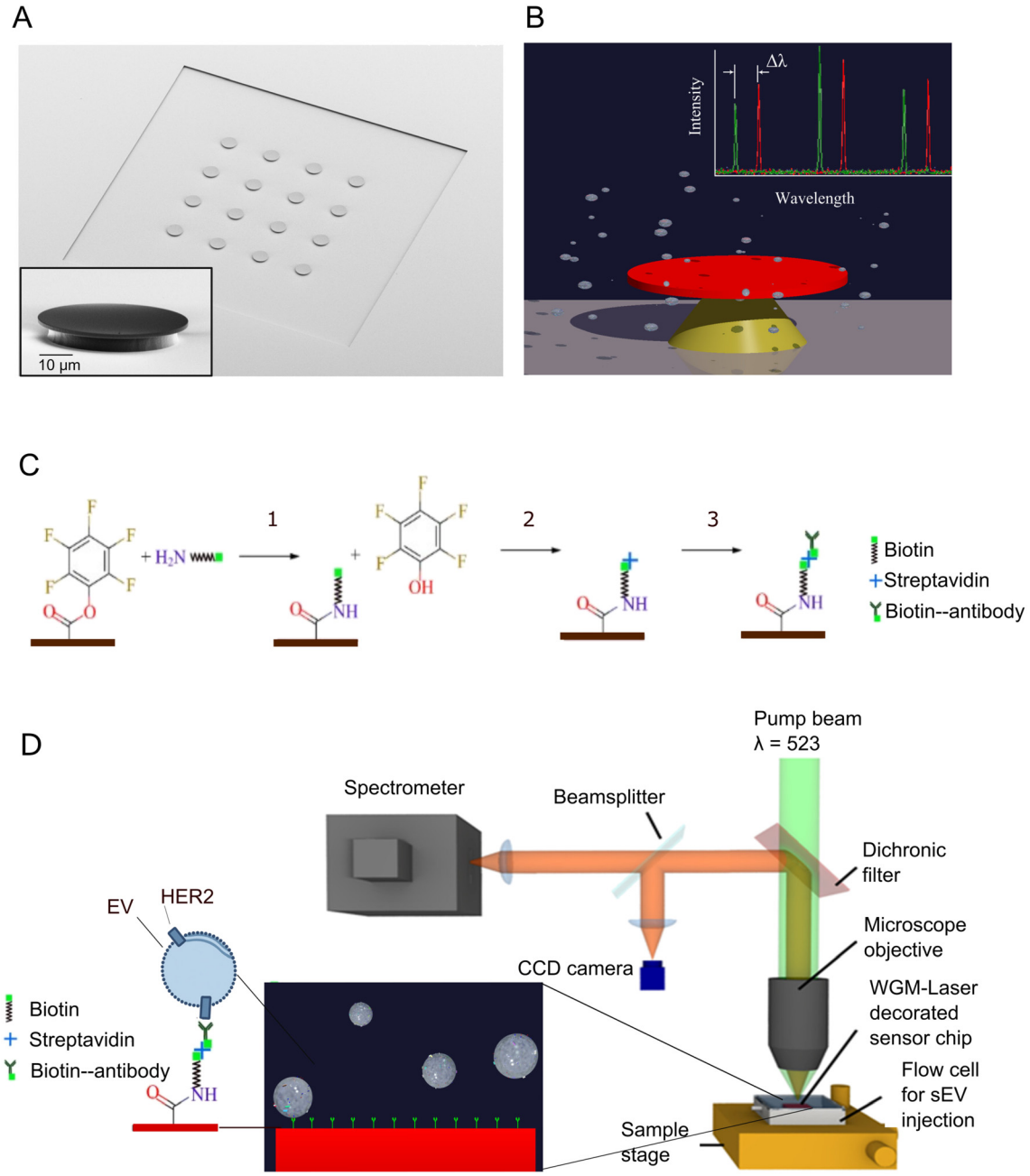

Fig. 1 WGM laser measurement setup. (A) Microscopy image of the sensor chip printed on a glass slide, supplemented with a whispering gallery mode (WGM) laser. The inset shows a single WGM laser (scale bar – 10 μm). (B) Schematic representation illustrating extracellular vesicles (EVs) approaching the surface of the WGM laser. This interaction causes a shift in the resonance intensity, observed as a change in wavelength ($\Delta\lambda$, red), enabling the detection of EV binding to the laser surface. (C) Surface functionalization protocol for EV detection. The surface modification follows a well-established three-step bioconjugation protocol: (1) activation of the sensor surface using chemical vapor deposition (CVD); (2) incubation with amine-terminated biotin to enable stable binding; (3) subsequent layering of streptavidin and biotinylated antibodies to ensure specific and oriented antibody presentation. (D) Scheme of the complete experimental setup. The WGM lasers are excited from above using a frequency-doubled pulsed Nd:YLF laser emitting at 523 nm (green). The pump beam is focused onto the sensor chip *via* a 20× microscope objective. The emitted light spectrum is captured using a spectrometer, and the lasing peaks are monitored using a dedicated algorithm. The sensor chip is mounted on a motorized stage, which follows a predetermined sequence to excite and measure multiple lasers simultaneously. The emission from the WGM lasers is collected through the same objective and directed to the acquisition system. Data acquisition is performed using a spectrometer (Shamrock 500i, iDUS, Andor), while part of the emission is routed to an auxiliary camera to monitor laser positions. The inset shows a magnified view of the WGM laser surface functionalized with antibodies that enable the specific EV binding for detection. For example, functionalization with HER2-specific antibodies allows the selective capture of HER2-positive EVs *via* antigen–antibody interactions on the laser surface, enabling their detection through spectral shifts.

binding induces a measurable spectral shift, which is recorded using a spectrometer (Fig. 1D).

2.2 Small extracellular vesicles (sEVs) exhibit high levels of HER2 full-length protein

The localization of HER2 on EVs has been previously described in a number of studies.[23–27] While these publications have explored a range of EV isolation techniques, they did not allow for a definitive conclusion regarding the HER2 presence in a distinct EV population or in different EV populations. To ascertain the HER2-positive EV population, we employed a differential centrifugation method to sequentially enrich EV of varying sizes, as previously outlined (Fig. S1).[34] The analysis encompassed crude fractions enriched in large EVs by sedimentation at 5000*g* (EV5) and 12 000*g* (EV12), along with small EVs (sEVs) enriched by ultracentrifugation at 120 000*g*. Initially,

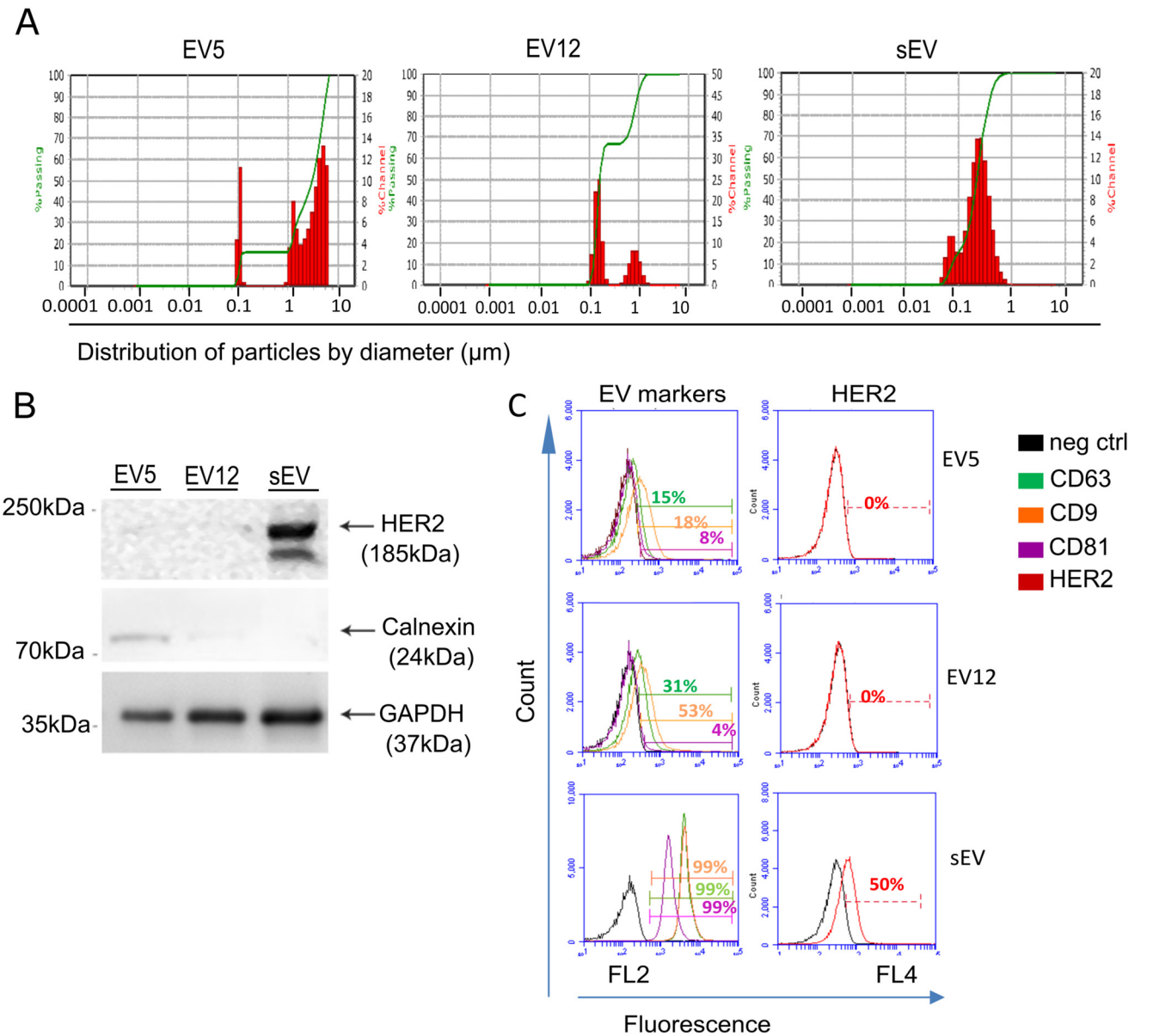

Fig. 2 Analysis of HER2 in different EV populations isolated from the cell culture supernatants. (A) Hydrodynamic size distribution of extracellular vesicles (EVs) enriched in different fractions (EV5, EV12, and sEVs), analyzed using dynamic light scattering (DLS). The data present the intensity distribution, providing better visualization of larger particles present in the fractions. (B) Western blot analysis of HER2 expression in different EV fractions. Protein samples (5 μg) from each EV fraction were loaded onto an SDS-PAGE gel for western blot analysis. A strong HER2-specific band is observed only in the sEV fraction, while calnexin, a marker for large vesicles, is predominantly detected in the EV5 fraction. GAPDH is included as a loading control. (C) Detection of HER2 and EV markers (CD63, CD9, and CD81) in different EV populations using bead-assisted flow cytometry. The negative control (neg ctrl) consists of sEVs coupled to beads and stained with an isotype control IgG and secondary antibody. Only the sEV fraction shows 50% of the population being positive for HER2. Analysis of other EV markers (CD63, CD9, and CD81) reveals weak presence in other EV fractions, whereas 99% of the sEV population exhibits a positive signal.

dynamic light scattering (DLS) was employed to characterize the size of particles present in the preparations. The resulting size distribution diagrams were generated based on particle brightness, revealing the presence of large particles ranging from 1 to 8 μm in EV5. In EV12, two distinct particle populations were identified: one between 0.1 and 0.5 μm, and another around 1 μm. In sEVs, a single population of particles with a peak at 0.1 μm was observed (Fig. 2A). The determined particle sizes corresponded to our expectations and to the published data;[34] we proceeded with the examination of the HER2 presence in different EV populations using western blotting. In consideration of the varying sizes of particles, equivalent protein quantities of EV5, EV12, and sEVs were loaded, irrespective of the particle number (Fig. 2B). Neither EV5 nor EV12 exhibited a HER2-specific band, whereas sEVs demonstrated a robust signal of the anticipated size. Additionally, calnexin was used as a marker for the endoplasmic reticulum, which can be present in vesicles shed directly from the cell membrane, but is not expected in exosomes derived from multivesicular bodies[1] and expected to be enriched in the sEV fraction. Consistently, a strong calnexin-specific signal was observed in EV5 and a faint band in EV12, while no calnexin signal was detected in sEVs (Fig. 2B, middle panel). To ensure the reliability of the results, GAPDH, utilized as a loading control, was examined. This analysis revealed comparable

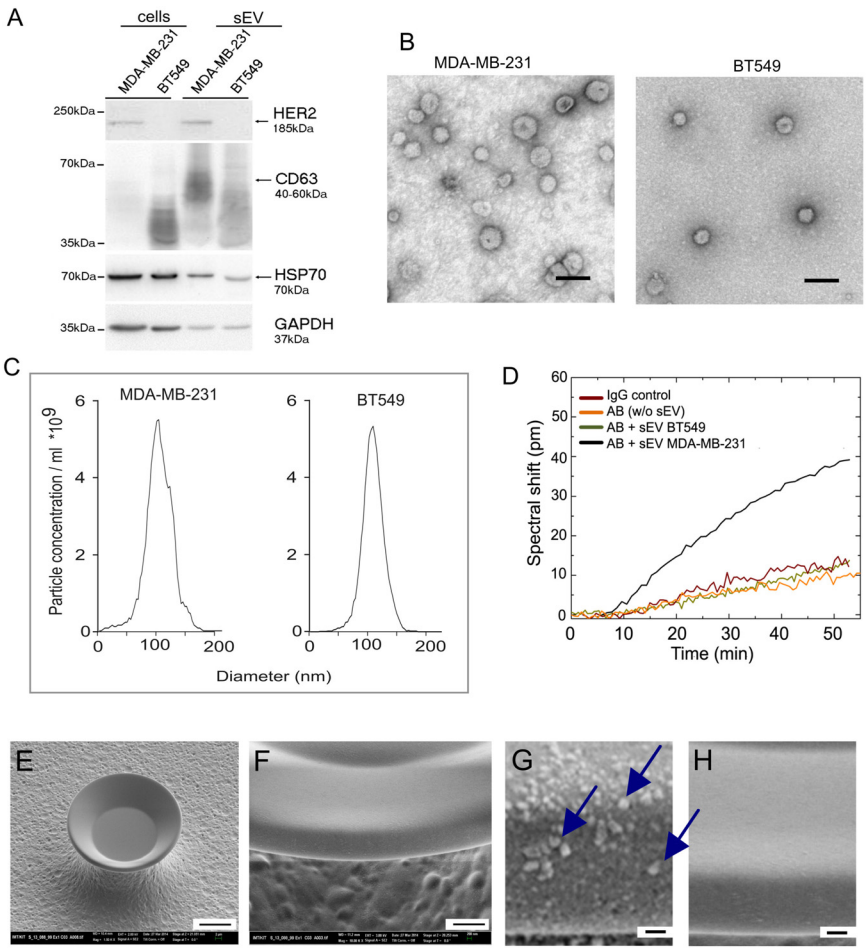

Fig. 3 Analysis of HER2+ and HER2− sEVs using the WGM laser. (A) HER2 expression in breast cancer cell lines MDA-MB-231 (HER2-positive) and BT549 (HER2-negative), as well as in their corresponding small extracellular vesicles (sEVs). For analysis, 10 μg of cell lysate and 2 μg of sEV samples were loaded onto an SDS-PAGE gel, followed by immunoblotting for HER2, the EV marker CD63, and loading controls HSP70 and GAPDH. (B) Transmission electron microscopy (TEM) image of the sEV preparations used in subsequent whispering gallery mode (WGM) laser detection experiments, confirming the integrity of isolated sEVs. Scale bar: 100 μm. (C) Size distribution of the prepared sEVs measured by nanoparticle tracking analysis (NTA), showing a consistent size distribution and a concentration of 5.7×10^9 particles per mL, prepared for WGM laser detection. (D) Initial WGM laser binding test using MDA-MB-231 sEVs on HER2-functionalized devices, showing a significant resonance shift (~40 pm) after 50 minutes (black line). Specificity of the observed signal was confirmed through three independent controls: HER2-negative BT549 sEVs (green line), antibody-only samples without EVs (orange line), and lasers functionalized with an isotype control incubated with MDA-MB-231 sEVs (IgG control, brown line). (E–H) Scanning electron microscopy (SEM) analysis of the WGM laser surface after EV incubation. (E) Overview image of the resonator. Scale bar: 10 μm; (F) digital enlargement of the resonator surface. Scale bar: 1 μm; (G) surface image showing round EV-like structures approximately 80 nm in diameter (blue arrows). Scale bar: 100 nm. (H) Control image of the resonator surface showing no EV-like structures. Scale bar: 100 nm.

protein levels in all three EV populations (Fig. 2B, bottom panel). Taking into account that HER2 undergoes proteolytic cleavage from the cell surface resulting in the release of the soluble HER2,[35] we determined if HER2 is exposed on the surface of EVs released by breast cancer cells. To this end, a bead-assisted flow cytometry approach was employed. In addition to HER2, EV-associated tetraspanins CD9, CD81, and CD63 were examined as positive controls. While EV5 and EV12 exhibited low levels of CD9, CD63, and CD81, and no expression of HER2 consistent with the WB data, sEVs were 99% positive for all three tetraspanins and 50% positive for HER2 (Fig. 2C). Consequently, the sEV fraction was considered to contain the majority of the membrane-bound HER2 in breast cancer cells and was selected for further examination.

2.3 WGM laser specifically detects HER2-positive sEVs

To demonstrate a proof-of-concept for EV detection using the WGM laser, we selected two breast cancer cell lines: HER2-expressing MDA-MB-231 and HER2-negative BT549. Initially, the presence of HER2 on sEVs was assessed *via* western blotting (Fig. 3A). In this analysis, CD63 was also examined as a universal EV biomarker expressed in both cell lines, while HSP70 and GAPDH served as loading controls (Fig. 3A, middle and bottom panels). The integrity and size distribution of sEVs were further evaluated using transmission electron microscopy (TEM) and nanoparticle tracking analysis (NTA), respectively. TEM revealed intact vesicles with diameters ranging from 50 to 90 nm (Fig. 3B), and the concentration of these vesicles was estimated by NTA to be 5.7×10^9 particles per mL for both cell lines (Fig. 3C).

Next, the ability of the WGM laser to detect HER2-positive sEVs was addressed. For that purpose, we decided to measure the development of the resonator spectral shift after loading the EV samples in real time (Fig. 3D). To achieve that, the laser set was fixed in a flow cell as shown in Fig. 1 and functionalized with either an anti-HER2 antibody or the corresponding isotype control (IgG) used as a negative control. Analytic solutions containing sEVs derived from MDA-MB-231 or BT549 cells were injected into the flow cell, and the spectral evolution of the lasing peaks over 50 min was tracked in each of the settings. Control samples without EVs showed a weak shift of 10 pm over the observation duration (Fig. 3D, orange line). A comparable shift was observed in different controls, including samples containing HER2-negative sEVs applied on a chip functionalized with HER2 antibody (Fig. 3D, green line), or HER2-positive sEVs applied on a chip functionalized with the isotype control (Fig. 3D, brown line). This non-zero shift, considered as a systematic error, or a background, caused by the referencing scheme used by the sensor, was identical for all control measurements. By sEV measurements, a long shift development up to 50 min was observed, which is unusual for single-molecule analytes, but seems to be common for EV measurements.[36] It is likely that it is due to a substantially larger size of sEVs as compared to the single molecule analytes, and a significantly longer period required for the signal development until final saturation and EV binding/diffusion rate balance. However, prolonged measurements were not feasible due to the photobleaching of the dyes used as dopants in the WGM laser. Their degradation led to an increased noise-to-signal ratio, compromising detection sensitivity. To visualize sEV bound to the surface of the WGM laser, scanning electron microscopy (SEM) was additionally performed (Fig. 3E–H), allowing the detection of EV-like structures of approximately 80 nm diameter on the WGM laser after adding sEVs (Fig. 3G and H), supporting the ability of the WGM laser to detect sEVs bound to the laser surface.

2.4 Detection limits of the WGM laser for sEV-associated HER2

In the previous section, the specificity of HER-2 functionalized sensors toward sEVs harbouring HER-2 was demonstrated. We then focused on determining the limit of detection (LOD) of the WGM laser by measuring the spectral shifts of sEV solutions with increasing concentrations, ranging from 0.7×10^7 to 21×10^7 [sEV per mL], over a period of 50 minutes, indicating that a loading of 1.4×10^7 EV per mL is sufficient to achieve a shift over the background (Fig. 4A). As a reference, conventional western blotting was employed (Fig. 4B), which demonstrated a sensitivity threshold at 1.7×10^8 particles, equivalent to 0.25 μg of the total EV protein amount. The analysis revealed WGM laser sensors exhibiting a sensitivity $S = 1.4 \times 10^7$ sEV per mL for detecting HER2-positive sEVs. Given the standard deviation of the lasing peaks ($\sigma = 0.45$ pm) and the relationship $\delta = 3\sigma/S$,[37] the limit of detection (LOD) was calculated to be approximately 10^7 sEV per mL (Fig. 4C).

To evaluate the performance of the WGM laser, we have summarized state-of-the-art methods recently reviewed elsewhere[38,39] in Table 1. The WGM laser platform achieves a competitive limit of detection (LOD) of $\sim 1.0 \times 10^7$ EV per mL, outperforming many broadly used techniques such as ELISA, NTA, and flow cytometry. Other emerging technologies developed in recent years, including on-chip surface plasmon resonance (SPR),[36] immunoelectrophoresis platform,[40] electrochemical immunoassay[41] and others[42,43] have demonstrated considerable potential for clinical application, particularly due to their ability to achieve very low detection limits, in some cases reaching as low as 10^5 EV per mL. However, their widespread application remains limited by high production costs and operational complexity, often requiring trained personnel and specialized infrastructure. In contrast, the WGM laser system presented here overcomes these challenges through the use of PDMS-based fabrication, which allows for rapid, scalable, and cost-effective production.

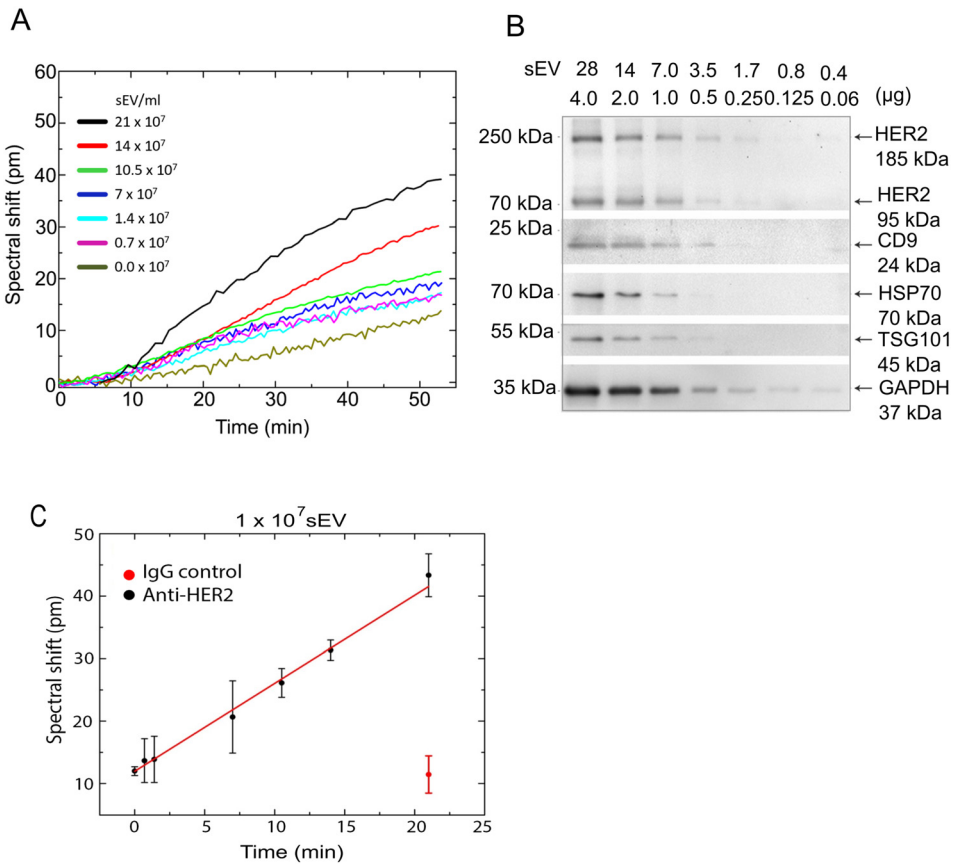

Fig. 4 Binding kinetics of sEVs and sensitivity of the WGM laser for HER2 detection. (A) Binding kinetics of varying sEV concentrations. The sensor response was evaluated across different sEV concentrations to determine sensitivity and detection limits. The resulting shifts were proportional to sEV concentrations, with a detection limit of 1×10^7 EV per mL in the injected sample. (B) Sensitivity analysis using conventional western blotting for HER2 detection in sEV preparation. At least 1.7×10^8 particles (corresponding to 0.125 μg of protein) were required to detect HER2 effectively, showing that the WGM laser has a 10 times greater sensitivity than the WB. (C) Sensitivity curve of the sensor. Each measurement exhibited a static additional positive shift of 10–12 pm caused by reference error, resulting in a non-zero baseline shift for zero concentration. For comparison, the response of the sensor to positive sEVs on isotype control antibody-functionalized surfaces is included (red data point). From the slope of the fitted line, the sensitivity was calculated as 1.4×10^7 sEV per mL, with a detection limit of approximately 1.0×10^7 sEV per mL. Error bars represent the standard deviations from at least three independent measurements.

Thus, the ongoing developments of diverse EV detection platforms—ranging from electrochemical sensors to advanced microfluidic and optical systems—represent a significant and positive evolution of the field. These technologies collectively offer complementary strengths and help address the varied demands of EV application in clinical diagnostics.

2.5 Selectivity of the WGM laser towards sEV-associated HER2

HER2 can be released from the cells through various molecular pathways as illustrated schematically in Fig. 5A. The soluble form of HER2, the so-called p105HER2 protein, can be detected by ELISA and is used in clinics as one of the biomarkers for the resistance towards HER2 targeted therapy.[44–46] In addition to this conventional release pathway, HER2 may also be secreted in its full-length form *via* incorporation into small extracellular vesicles (sEVs). Unlike the cleaved soluble form, the detection of full-length, membrane-bound HER2 on EVs could suggest that the originating tumor cells retain the intact protein and may remain responsive to HER2-targeted treatment.

Thus, most likely, the soluble and the EV-bound HER2 have opposite clinical indications. We propose that distinguishing between soluble and EV-associated HER2 could offer additional value as a potential indicator of therapeutic responsiveness in the context of HER2-targeted cancer therapies.

Therefore, we asked if WGM lasers are capable of distinguishing between soluble HER2 and EV-bound HER2. We tested the sensitivity of WGM lasers towards the cleaved extracellular domain (ECD) of HER2 *versus* full length EV-bound HER2. For that purpose, the recombinant HER2 protein (rHER2) consisting of the HER2 extracellular domain, was applied. First, we demonstrated using western blotting that the antibody used to functionalize WGM lasers recognized both the membrane-bound HER2 located on sEVs and the soluble ECD of HER2. For that,

Table 1 State of the art technologies for EV biomarker detection

Technology	LOD	Sample volume	EV HER2 specificity	Throughput	Strengths	Limitations
WGM laser (this work)	~1.0×10^7 sEV per mL	10 μL	Yes (full-length HER2 only)	Moderate	Label-free, high specificity, membrane HER2 discrimination	Photobleaching limits long-term observation
Electrochemical biosensor	4.7×10^5 EV per μL (= 4.7×10^8 mL^{-1})	10 μL	Yes (soluble HER2 detection)	High	Good sensitivity, aptamer- or antibody-based selectivity	Requires complex nanomaterial prep, limited to soluble HER2
ELISA	~10^8–10^9 EV per mL	50–100 μL	Partial (no membrane-bound HER2 discrimination)	Moderate	Standardized, high reproducibility	No distinction between soluble and vesicle-associated HER2
Flow cytometry	~10^7–10^8 EV per mL	100 μL	Yes (if pre-sorted)	High	Single-vesicle analysis, multiplexing	Requires labeling, large sample volume
NTA	~10^7–10^8 EV per mL	500 μL	No	Low	Size/concentration profiling	Cannot distinguish EV origin or biomarkers
TRPS	~10^7 EV per mL	40 μL	No	Low–moderate	Size/count with pore tuning	No biomarker data
Microfluidics (*e.g.* ExoChip, ExoSearch, nPLEX)	10^6–10^7 EV per mL	10–50 μL	Yes (depends on antibody)	Moderate–high	Low sample volume, multiplexing possible, automation-friendly	Complexity in chip fabrication, limited standardization
Nano-flow cytometry [*e.g.* PMID: 33895846]	~1.0×10^7 EV per mL	10–50 μL	Yes (surface labeling)	High	Improved resolution for particles <200 nm, single-EV analysis	Requires fluorescent tags; still emerging for clinical routine
Fluorescent NTA	~1.0×10^7–10^8 EV per mL	500 μL	No	Low	Good for size/concentration profiles	No molecular specificity; dye bleaching limits fluorescence mode
TRPS (qNano)	~1.0×10^7 EV per mL	40 μL	No	Low–moderate	Accurate size/count, tunable pore geometry	Lacks marker-specific information
Surface plasmon resonance (SPR)	~1.0×10^6–10^7 EV per mL	10–20 μL	Yes (*via* capture antibody)	Moderate	Label-free, real-time detection, kinetic analysis	Requires stable surface chemistry and chip regeneration

5 μg of rHER2 protein was loaded on the gel. Additionally, MDA-MB-231-derived EVs were used as a positive control and the BT549-derived EVs as a negative control. The antibody was able to detect both the recombinant protein, visualized at a size of 95 kDa, and the full length sEV-associated HER2, visualized as a 185 kDa band in MDA-MB-231 sEVs (Fig. 5B).

Then, the ability of sensors to detect rHER2 protein was tested. For that, rHER2 dissolved in 1× PBS with a concentration of 5 μg mL^{-1} was used to react with the sensors. Importantly, this concentration exceeds the recommended threshold for breast cancer detection by more than 300-fold, with a cut-off value of 15 ng mL^{-1} as recommended by the FDA.[46] Additionally, EVs derived from MDA-MB-231 and BT549 were tested with lasers functionalized with either HER2 antibody or CD63 antibody used as a universal EV biomarker, and with an IgG isotype control.

Neither rHER2 nor BT459 sEVs showed a shift over the negative control samples containing PBS and the isotype control, if tested with the HER2-functionalized laser (Fig. 5C, brown and orange bars, respectively). The shift was visible exclusively with the lasers functionalized with HER2 antibody, if the sEVs derived from the MDA-MB-231 cells were added (Fig. 5C, orange bars), and with the lasers functionalized with the CD63 antibody and incubated with sEVs derived from the BT549 or MDA-MB-231 cells both positive for CD63 (Fig. 5C, blue bars). These data support that the WGM laser application established in this work allows for a specific recognition of EV biomarkers.

2.6 WGM-laser successfully detects sEV-associated HER2 in patients' serum samples outperforming gold standard techniques

We previously demonstrated the specificity of WGM lasers for detecting EV-associated HER2 using cell culture-derived samples. Here, we evaluated their ability to recognize HER2 on EVs isolated from serum samples of breast cancer patients. Serum samples were processed using the same experimental scheme as the cell culture supernatant (Fig. S1). Thus, EV5 population was enriched by centrifugation at 5000*g*, the EV12 was enriched by centrifugation at 12 000*g* (EV12), and sEVs were enriched by ultracentrifugation at 120 000*g*. To characterize particle sizes within these fractions, we utilized dynamic light scattering (DLS), as nanoparticle tracking analysis (NTA) does not fully cover the expected size range of 10 nm–10 μm and has limitations to measure highly heterogeneous mixtures.[47–49] Generated crude EV fractions were expected to contain high amounts of different lipoproteins, protein complexes, and residual platelets, besides EVs.[18,50–52] However, it was an important prerequisite

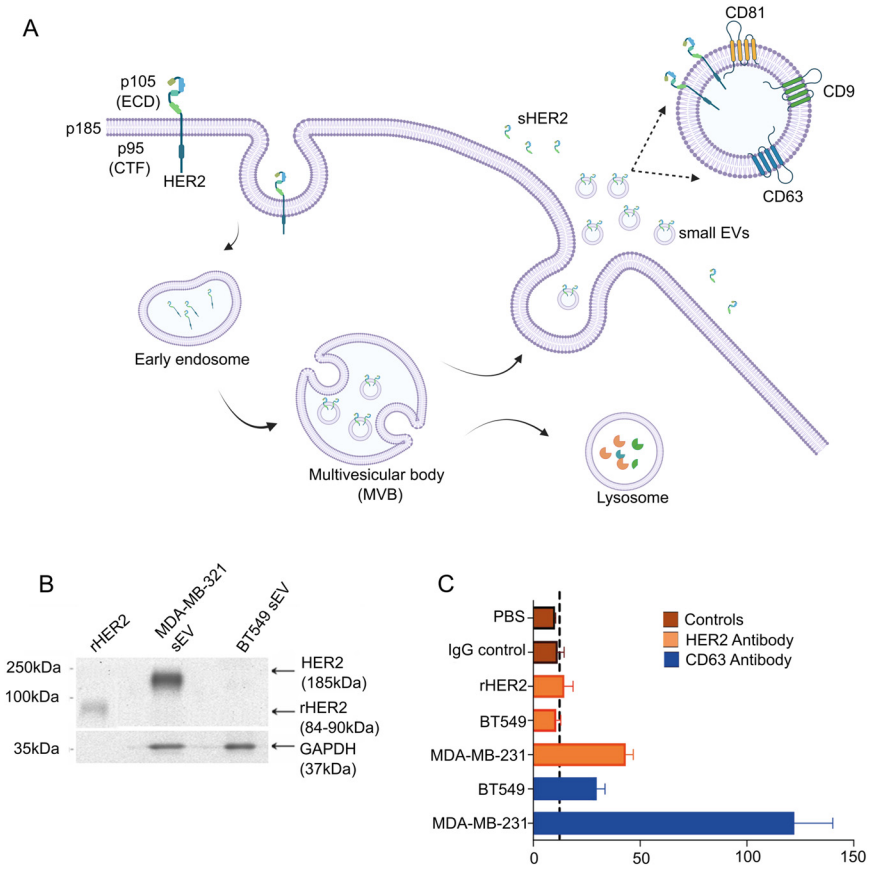

Fig. 5 Selectivity of the WGM resonator for the detection of the sEV-bound HER2. (A). Schematic representation of HER2 release pathways. This includes the release of the truncated extracellular domain p105HER2 and full-length HER2 integrated into the membranes of small extracellular vesicles (sEVs). (B). Western blot analysis demonstrating the ability of the antibody (AB) used for functionalizing the resonators to specifically recognize recombinant HER2 (rHER2), corresponding to the HER2 extracellular domain (ECD) released after cleavage into the extracellular space. (C). Detection of sEVs derived from BT549 and MDA-MB-231 cell lines using WGM lasers functionalized with either CD63 (blue bars) or HER2 antibodies (orange bars). While CD63 is present on both the BT549 and MDA-MB-231 EVs, it serves as a positive control for BT549 sEVs. For each measurement, 1×10^8 EVs were incubated on the chip containing WGM lasers for 50 minutes. The data provide a proof of concept that the laser selectively detects only EV-bound HER2, but not the soluble recombinant protein.

to use the WGM-laser on EV samples containing a certain proportion of non-EV components, as the preparation of highly pure EVs from blood samples is laborious, has low recovery, and is barely applicable in clinical routine.[18,52,53]

We assumed that the presence of non-EV particles should not affect the detection power of the laser as unbound particles are removed by washing steps as described in the Methods section.

DLS analysis revealed a broad size distribution in the EV5 fraction, ranging from 10 nm to 5 μm. The EV12 fraction exhibited two dominant populations at ~10 nm and ~100 nm, while the sEV fraction was enriched in smaller particles, likely lipoproteins (~10 nm), along with a population of ~100 nm particles, which may consist of lipoproteins and EVs (Fig. 6A, Table S1). The presence of EV biomarkers was examined by bead-assisted flow cytometry. Using the universal biomarkers CD9, CD63, and CD81 together with HER2, all fractions were tested. Consistent with the results observed by the analysis of the cell culture-derived samples, the sEV fraction exhibited the highest levels of these proteins (Fig. 6B). Consequently, the sEVs were selected for further analysis and were enriched by differential centrifugation from the serum of 10 patients with breast cancer and two healthy female donors. The samples were characterized using standard methods including bicinchoninic acid assay (BCA) and nanoparticle tracking analysis (NTA), showing a comparable size and particle number in the sEV-enriched fractions ranging between 6.4×10^9 and 14.2×10^9 particles of approximately 130 nm diameter isolated from 1 mL of blood serum (Tables S1 and S2; Fig. S3 and S4).

Patient-derived sEV samples were analyzed using WGM lasers functionalized with a HER2-specific antibody. For each measurement, 15 μL of the sEV fraction isolated from the serum was diluted in 985 μL of PBS and applied to the sensor chip. The resulting spectral shifts were then compared to two parameters: the total EV particle count (Fig. 6C) and HER2 concentration measured by ELISA, which is currently considered the clinical gold standard for HER2 quantification (Fig. 6D; Table S2). For the ELISA, 100 μL of each sEV sample was used.

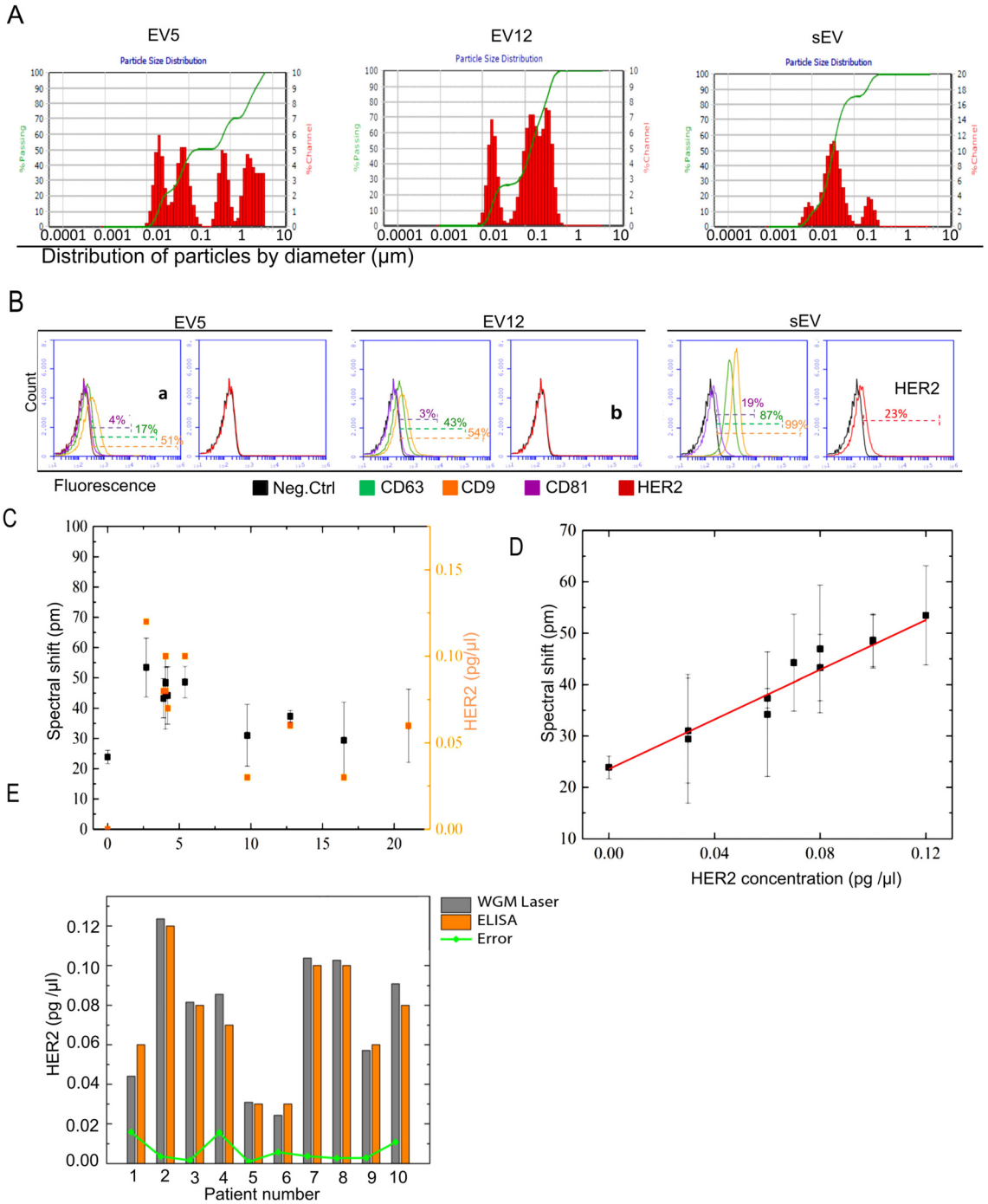

Fig. 6 WGM laser measurement of HER2 in patient samples. (A) Hydrodynamic size distribution of extracellular vesicles (EVs) enriched from the serum of a breast cancer patient in different fractions (EV5, EV12, and sEVs), analyzed using dynamic light scattering (DLS). The intensity distribution highlights the presence of larger particles in the fractions. (B) Detection of HER2 and EV markers (CD63, CD9, and CD81) in different EV populations using bead-assisted flow cytometry. The negative control (neg ctrl) consists of sEVs coupled to beads and stained with an isotype control IgG and secondary antibody. Only the sEV fraction shows 23% of the population positive for HER2. CD63 and CD9 are detectable in EV5 and EV12 fractions, whereas CD81 is predominantly found in sEVs. (C) Comparison of WGM laser and ELISA measurements for HER2 detection relative to the total number of sEVs. The spectral shifts are independent of the total number of sEVs, as only a small fraction of sEVs is HER2-positive, and this proportion varies between patients. Notably, a similar trend is observed in the ELISA measurements. (D) A stronger correlation is observed between the WGM laser spectral shifts and HER2 content measured by ELISA. The dependence is modeled using a linear fit. (E) A calibration function is derived from the linear fit equation to interpret spectral shifts and visualize the correlation between the WGM laser and ELISA approaches. This demonstrates that WGM lasers provide diagnostic results comparable to established techniques, requiring minimal sample volume. Error bars represent the standard deviation from at least three independent measurements.

While no correlation was observed between the total EV particle number and the WGM signal (Fig. 6C), a clear linear correlation was found between the WGM spectral shift and the HER2 concentration determined by ELISA (Fig. 6D). Based on this correlation, a calibration function was derived to quantitatively interpret the WGM shifts (Fig. 6E), demonstrating the consistency and reliability of the WGM readout. Notably, when comparing the sample input required for HER2 detection, the WGM-based method demonstrated superior analytical sensitivity relative to ELISA. In our experiments, ELISA required approximately 1×10^8 EVs to produce a detectable HER2 signal, whereas the WGM laser platform achieved reliable detection with only 1×10^7 EVs. These findings are consistent with the published performance data summarized in Table 1 and reflect a tenfold improvement in the limit of detection using the WGM approach.

3. Conclusions

We successfully demonstrated a new approach for detecting EV-associated HER2 in human serum, enabling accurate quantification that outperforms the current gold standard in sensitivity. This assay holds strong potential as an independent tool for monitoring HER2 levels in breast cancer patients, particularly in the context of ongoing therapy. Looking ahead, the integration of WGM laser sensors into multiplexed chip-based arrays could enable the simultaneous detection of multiple EV biomarkers from minimal sample volumes. More broadly, the adoption of WGM laser technology – or comparable label-free platforms – as a core component of diagnostic strategies could transform the clinical management of HER2-expressing tumors. The ability to directly selectively membrane-bound HER2 – an option not available with current standard methods – could open new avenues for precision oncology. However, realizing this potential will require further clinical validation, which lies beyond the scope of the present study.

4. Methods

Isolation of extracellular vesicles (EVs)

Small extracellular vesicles (sEVs) were isolated from cell lines and patient sera using differential centrifugation. Blood samples from breast cancer patients were obtained from the Department of Obstetrics and Gynecology at the Medical Center, University of Freiburg. All experiments were performed in accordance with the Guidelines of Declaration of Helsinki. Experiments and the study protocol (36/12) were approved by the ethics committee at the Albert-Ludwigs-University of Freiburg, Germany. Informed consents were obtained from human participants of this study. Blood collected in vacutainers was centrifuged at 2500 × *g* for 20 minutes to obtain serum, which was subsequently stored at −80 °C until further processing. Centrifugation was performed at 2500 ×g for 15 minutes to remove cell debris, followed by 5000 × *g* for 45 minutes and 12 000 × *g* for 30 minutes, yielding intermediate fractions (EV5 and EV12). A final ultracentrifugation step at 120 000 × *g* for 70 minutes produced the fraction enriched in small EVs (sEVs). The pellets were washed in 1× PBS and with a repeated ultracentrifugation step, then resuspended in 1× PBS and used for further characterization and analysis.

Nanoparticle tracking analysis (NTA)

Nanoparticle tracking analysis (NTA) was used to determine the size distribution and concentration of sEVs. The samples were measured with ZetaView® PMX 110 V3.0 from Particle Metrix using the software ZetaView 8.4.2. Before each measurement, the instrument was calibrated using 100 nm standard polystyrene beads (at a ratio of 1 : 125 000) supplied by the company. The parameters were pre-set during measurement in the automated software with a shutter speed of 70 and a frame rate of 30 frames per second (fps). The samples were diluted in 0.1% PBS (cell derived EVs) and 0.1% HEPES (patient derived EVs). 1 mL of diluted sample was injected into the cell for measurement. The dilution of the sample was appropriately adjusted to maintain the sensitivity at 85–90 for all samples. The post-acquisition parameters were set to min size: 5, max size: 1000, and min brightness: 20. For patient derived EVs, min size: 5, max size: 255, and min brightness: 20. For determining the size distribution, each sample was measured at 11 different positions (5 cycles) with the removal of any outlier positions (at least 8 positions were used in each measurement).

Dynamic light scattering (DLS)

In order to determine the hydrodynamic size distribution of particles present in the EV5, EV12, and sEV samples, DLS was employed. 10 μL of the sample were measured using a NANO-flex 180° particle size analyzer (Particle Metrix, Meerbusch, Germany) according to manufacturer's guidelines. The system detects size distribution in the range of 30 nm–10 μm and is based on the heterodyne 180° backscattering principle. The viscosity and refractive index were set according to the buffer used. In the case of cell-derived EVs, PBS was used, while for patient-derived EVs, HEPES buffer was used. The measurements were analyzed using the software – MicrotracFLEX 11.0.0.5.

Bead-assisted flow cytometry

To measure biomarker expression on EVs, bead-assisted flow cytometry was employed. For this, 1×10^9 EVs were incubated with 4 μm aldehyde/sulphate latex beads for 15 minutes at room temperature (RT) to enable detection by the flow cytometer. The free aldehyde and sulfate groups on the beads were blocked by incubating with 100 μL of 1 M glycine/PBS and 100 μL of 10% BSA/PBS at RT for 30 minutes. The latex beads were then pelleted by centrifugation at 10 000*g* for 2 minutes at RT, and the supernatant was discarded. After two washes with 3% BSA/PBS, the beads were incubated with 20 μL of primary

antibody for 1 hour at 4 °C. Following this, they were incubated with a secondary antibody for 30 minutes at 4 °C, followed by two washes with 3% BSA/PBS. After discarding the supernatant, the pellet was resuspended in 300 μL of 3% BSA/PBS for measurement. The samples were analyzed using a BD Accuri™ C6 flow cytometer, with the data analyzed using BD CSampler™ software. A threshold of 80 000 FSC-H (T1) and 10 SSC-H (T2) was applied for measurement. A total of 100 000 events were recorded per sample at medium core speed.

Protein quantification

The sEV protein concentration was determined using a Micro BCA™ protein assay kit (Thermo Scientific) according to the manufacturer's guidelines with a detection limit of 0.5 to 20 micrograms per mL.

ELISA

The HER2 levels in sEVs from breast cancer patients were determined using the 'Human ErbB2/Her2 Quantikine ELISA' kit (R&D Systems) according to the manufacturer's guidelines. Briefly, the ELISA standards provided with the kit and 50 μL of sEV samples were loaded onto a 96-well microplate pre-coated with monoclonal antibody specific to human HER2. After incubation, the unbound substances were washed away with a wash buffer provided with the kit, and an enzyme-linked polyclonal antibody specific to HER2 was added to the wells. After the washing step, the substrate solution was added leading to color development. After 30 min, the color development was stopped, and the optical density was measured at 450 nm using a TECAN microplate reader. The standard curve was generated with the ELISA standards using Microsoft Excel 2010 (Microsoft Corp., Seattle, WA, USA).

Fabrication of WGM laser arrays

The fabrication process of the laser array follows a previously established method.[29,33] In the first step, a 5 μm-thick layer of polymethylglutarimide (PMGI, MicroChem Corp.) was spin-coated onto a silicon wafer. In the second step, a 1.2 μm-thick layer of polymethyl methacrylate (PMMA, MicroChem Corp.) mixed with pyrromethene 597 (Radiant Dyes Laser & Accessories GmbH) was spin-coated over the PMGI layer. The coated wafer was then patterned using electron beam lithography, followed by the development of the PMMA layer in a 1 : 1 mixture of methyl isobutyl ketone (MIBK) and isopropanol (IPA) to define arrays of disk structures. The PMGI layer was then subjected to isotropic wet etching with a 101A developer (MicroChem), which underetches the PMMA disks, creating pedestals and thereby freeing the edges of the disks, where whispering-gallery modes can propagate. Finally, the wafer was diced to separate the sensor arrays.

Surface activation and functionalization of WGM laser arrays

The sensor chips were surface-activated by depositing a poly(*p*-xylylene) layer functionalized with pentafluorophenyl (PFP) ester groups, using chemical vapor deposition (CVD) of [2.2]paracyclophane-4-carboxylic acid pentafluorophenyl ester. PFP-ester-functionalized surfaces can then be reacted *via* click chemistry, enabling the attachment of a variety of receptor molecules terminated with amino groups.[54] Following surface activation, a subset of sensors within the array was passivated by applying a thick layer of index-matched UV-curable adhesive (MY136 V2000, MYpolymers LTD, Israel). These passivated lasers serve as references to correct for artifacts in the sensor signal, such as those arising from temperature drift and the photobleaching of pyrromethene 597, as previously described.[29] To functionalize the unpassivated lasers, chips coated with PFP-ester groups and selectively passivated were first incubated in a 500 μM solution of amine-terminated biotin for 24 hours. This incubation period not only allows the surface-binding reaction to reach chemical equilibrium, but also ensures that the laser swelling saturates, preventing interference with the detection signal. Following this, the sensors were incubated for 30 minutes in a 500 nM solution of streptavidin, which binds to the biotin and acts as a cross-linker for the next functionalization layer. The final step involved incubating the sensors in a biotinylated antibody solution for 30 minutes. The biotin binds to the surface-immobilized streptavidin, thereby anchoring the antibody to the surface (Fig. 1C).

WGM laser spectrum measurement

The measurement setup is described in detail (Fig. S2).[29] The WGM lasers are pumped by a frequency-doubled pulsed Nd:YLF laser emitting at 523 nm. The laser beam is focused onto the sensors using a microscope objective (20×, NA = 0.42). The sensor chip is positioned in a flow cell, which is mounted on an automated sample stage. This setup allows for precise, sequential movements to repeatedly pump and measure a specific selection of lasers. Emission from the WGM lasers is collected through the same objective lens and directed to the acquisition system. Data acquisition is performed using a Czerny–Turner monochromator (Shamrock 500i, Andor) coupled with a CCD camera (iDus, Andor). The emission spectra are analyzed with dedicated software to monitor the evolution of the peak positions over time.

Scanning electron microscopy (SEM)

After incubation with HER2-positive EVs, the WGM laser chip was rinsed gently with PBS to remove unbound particles. The chip was then fixed with 2.5% glutaraldehyde in PBS for 30 minutes at room temperature. Following fixation, the chip was washed thoroughly with PBS and subjected to sequential dehydration by immersion in increasing concentrations of ethanol (30%, 50%, 70%, 90%, and 100%) for 10 minutes at each concentration. The chip was subsequently air-dried

completely in a dust-free environment. Once dried, the chip was mounted onto SEM stubs using conductive adhesive tape. To enhance conductivity and improve image quality, the sample was sputter-coated with a thin layer of gold (3–5 nm). For SEM imaging, parameters were optimized to capture high-quality images at various magnifications, ensuring detailed visualization of the chip surface and EV morphology.

Author contributions

S. F. W., M. H., C. K.: planning of experiments, WGM sensor fabrication, biosensing measurements under supervision of C. K. R. K.: planning and carrying out the experiments for EV isolation and characterization, contributing to manuscript writing. I. N.: project planning, manuscript writing. A. H.: localized passivation. C. H., M. K., J. L.: PFP ester synthesis and coating. D. K., S. Kr., H. K., W. F.: discussion, planning of WGM experiments and supervision. U. B., T. W., S. Kö., T. M.: discussion, planning of initial WGM experiments.

Conflicts of interest

Irina Nazarenko is the co-founder and chief scientific officer of CapCo Bio GmbH.

Data availability

The data supporting this article have been included as part of the supplementary information (SI). Supplementary information: this supplementary material provides additional details to EV isolation protocol, sensor principles, protein and nanoparticle analyses, and clinical characterization data supporting the detection of HER2-positive extracellular vesicles using WGM resonator-based liquid biopsy technology See DOI: https://doi.org/10.1039/d5lc00269a.

Acknowledgements

This work was carried out with the support from the Karlsruhe Nano Micro Facility (KNMF), a Helmholtz Research Infrastructure at Karlsruhe Institute of Technology, the EV-Core Research Infrastructure RI_00612 supported by Deutsche Forschungsgemeinschaft and the Medical Faculty of University of Freiburg; Alfried Krupp von Bohlen und Halbach Foundation; European Research Council (ERC Starting Grant 'EnTeraPIC', number 280145); Karlsruhe School of Optics and Photonics (KSOP), Horizon 2020 EIC project NEXUS grant No 101058200 and BMFTR grant 03ZU1208CA nanodiag_BW, and BMFTR grant 13GW060F EV-Surf.

References

1 M. Yanez-Mo, P. R. Siljander, Z. Andreu, A. B. Zavec, F. E. Borras, E. I. Buzas, K. Buzas, E. Casal, F. Cappello, J. Carvalho, E. Colas, A. Cordeiro-da Silva, S. Fais, J. M. Falcon-Perez, I. M. Ghobrial, B. Giebel, M. Gimona, M. Graner, I. Gursel, M. Gursel, N. H. Heegaard, A. Hendrix, P. Kierulf, K. Kokubun, M. Kosanovic, V. Kralj-Iglic, E. M. Kramer-Albers, S. Laitinen, C. Lasser, T. Lener, E. Ligeti, A. Line, G. Lipps, A. Llorente, J. Lotvall, M. Mancek-Keber, A. Marcilla, M. Mittelbrunn, I. Nazarenko, E. N. Nolte-'t Hoen, T. A. Nyman, L. O'Driscoll, M. Olivan, C. Oliveira, E. Pallinger, H. A. Del Portillo, J. Reventos, M. Rigau, E. Rohde, M. Sammar, F. Sanchez-Madrid, N. Santarem, K. Schallmoser, M. S. Ostenfeld, W. Stoorvogel, R. Stukelj, S. G. Van der Grein, M. H. Vasconcelos, M. H. Wauben and O. De Wever, *J. Extracell. Vesicles*, 2015, **4**, 27066, DOI: 10.3402/jev.v4.27066.

2 C. Thery, K. W. Witwer, E. Aikawa, M. J. Alcaraz, J. D. Anderson, R. Andriantsitohaina, A. Antoniou, T. Arab, F. Archer, G. K. Atkin-Smith, D. C. Ayre, J. M. Bach, D. Bachurski, H. Baharvand, L. Balaj, S. Baldacchino, N. N. Bauer, A. A. Baxter, M. Bebawy, C. Beckham, A. Bedina Zavec, A. Benmoussa, A. C. Berardi, P. Bergese, E. Bielska, C. Blenkiron, S. Bobis-Wozowicz, E. Boilard, W. Boireau, A. Bongiovanni, F. E. Borras, S. Bosch, C. M. Boulanger, X. Breakefield, A. M. Breglio, M. A. Brennan, D. R. Brigstock, A. Brisson, M. L. Broekman, J. F. Bromberg, P. Bryl-Gorecka, S. Buch, A. H. Buck, D. Burger, S. Busatto, D. Buschmann, B. Bussolati, E. I. Buzas, J. B. Byrd, G. Camussi, D. R. Carter, S. Caruso, L. W. Chamley, Y. T. Chang, C. Chen, S. Chen, L. Cheng, A. R. Chin, A. Clayton, S. P. Clerici, A. Cocks, E. Cocucci, R. J. Coffey, A. Cordeiro-da-Silva, Y. Couch, F. A. Coumans, B. Coyle, R. Crescitelli, M. F. Criado, C. D'Souza-Schorey, S. Das, A. Datta Chaudhuri, P. de Candia, E. F. De Santana, O. De Wever, H. A. Del Portillo, T. Demaret, S. Deville, A. Devitt, B. Dhondt, D. Di Vizio, L. C. Dieterich, V. Dolo, A. P. Dominguez Rubio, M. Dominici, M. R. Dourado, T. A. Driedonks, F. V. Duarte, H. M. Duncan, R. M. Eichenberger, K. Ekstrom, S. El Andaloussi, C. Elie-Caille, U. Erdbrugger, J. M. Falcon-Perez, F. Fatima, J. E. Fish, M. Flores-Bellver, A. Forsonits, A. Frelet-Barrand, F. Fricke, G. Fuhrmann, S. Gabrielsson, A. Gamez-Valero, C. Gardiner, K. Gartner, R. Gaudin, Y. S. Gho, B. Giebel, C. Gilbert, M. Gimona, I. Giusti, D. C. Goberdhan, A. Gorgens, S. M. Gorski, D. W. Greening, J. C. Gross, A. Gualerzi, G. N. Gupta, D. Gustafson, A. Handberg, R. A. Haraszti, P. Harrison, H. Hegyesi, A. Hendrix, A. F. Hill, F. H. Hochberg, K. F. Hoffmann, B. Holder, H. Holthofer, B. Hosseinkhani, G. Hu, Y. Huang, V. Huber, S. Hunt, A. G. Ibrahim, T. Ikezu, J. M. Inal, M. Isin, A. Ivanova, H. K. Jackson, S. Jacobsen, S. M. Jay, M. Jayachandran, G. Jenster, L. Jiang, S. M. Johnson, J. C. Jones, A. Jong, T. Jovanovic-Talisman, S. Jung, R. Kalluri, S. I. Kano, S. Kaur, Y. Kawamura, E. T. Keller, D. Khamari, E. Khomyakova, A. Khvorova, P. Kierulf, K. P. Kim, T. Kislinger, M. Klingeborn, D. J. Klinke, , 2nd, M. Kornek, M. M. Kosanovic, A. F. Kovacs, E. M. Kramer-Albers, S. Krasemann, M. Krause, I. V. Kurochkin, G. D. Kusuma, S. Kuypers, S. Laitinen, S. M. Langevin, L. R. Languino, J. Lannigan, C. Lasser, L. C. Laurent, G. Lavieu, E. Lazaro-

Ibanez, S. Le Lay, M. S. Lee, Y. X. F. Lee, D. S. Lemos, M. Lenassi, A. Leszczynska, I. T. Li, K. Liao, S. F. Libregts, E. Ligeti, R. Lim, S. K. Lim, A. Line, K. Linnemannstons, A. Llorente, C. A. Lombard, M. J. Lorenowicz, A. M. Lorincz, J. Lotvall, J. Lovett, M. C. Lowry, X. Loyer, Q. Lu, B. Lukomska, T. R. Lunavat, S. L. Maas, H. Malhi, A. Marcilla, J. Mariani, J. Mariscal, E. S. Martens-Uzunova, L. Martin-Jaular, M. C. Martinez, V. R. Martins, M. Mathieu, S. Mathivanan, M. Maugeri, L. K. McGinnis, M. J. McVey, D. G. Meckes Jr., K. L. Meehan, I. Mertens, V. R. Minciacchi, A. Moller, M. Moller Jorgensen, A. Morales-Kastresana, J. Morhayim, F. Mullier, M. Muraca, L. Musante, V. Mussack, D. C. Muth, K. H. Myburgh, T. Najrana, M. Nawaz, I. Nazarenko, P. Nejsum, C. Neri, T. Neri, R. Nieuwland, L. Nimrichter, J. P. Nolan, E. N. Nolte-'t Hoen, N. Noren Hooten, L. O'Driscoll, T. O'Grady, A. O'Loghlen, T. Ochiya, M. Olivier, A. Ortiz, L. A. Ortiz, X. Osteikoetxea, O. Ostergaard, M. Ostrowski, J. Park, D. M. Pegtel, H. Peinado, F. Perut, M. W. Pfaffl, D. G. Phinney, B. C. Pieters, R. C. Pink, D. S. Pisetsky, E. Pogge von Strandmann, I. Polakovicova, I. K. Poon, B. H. Powell, I. Prada, L. Pulliam, P. Quesenberry, A. Radeghieri, R. L. Raffai, S. Raimondo, J. Rak, M. I. Ramirez, G. Raposo, M. S. Rayyan, N. Regev-Rudzki, F. L. Ricklefs, P. D. Robbins, D. D. Roberts, S. C. Rodrigues, E. Rohde, S. Rome, K. M. Rouschop, A. Rughetti, A. E. Russell, P. Saa, S. Sahoo, E. Salas-Huenuleo, C. Sanchez, J. A. Saugstad, M. J. Saul, R. M. Schiffelers, R. Schneider, T. H. Schoyen, A. Scott, E. Shahaj, S. Sharma, O. Shatnyeva, F. Shekari, G. V. Shelke, A. K. Shetty, K. Shiba, P. R. Siljander, A. M. Silva, A. Skowronek, O. L. Snyder 2nd, R. P. Soares, B. W. Sodar, C. Soekmadji, J. Sotillo, P. D. Stahl, W. Stoorvogel, S. L. Stott, E. F. Strasser, S. Swift, H. Tahara, M. Tewari, K. Timms, S. Tiwari, R. Tixeira, M. Tkach, W. S. Toh, R. Tomasini, A. C. Torrecilhas, J. P. Tosar, V. Toxavidis, L. Urbanelli, P. Vader, B. W. van Balkom, S. G. van der Grein, J. Van Deun, M. J. van Herwijnen, K. Van Keuren-Jensen, G. van Niel, M. E. van Royen, A. J. van Wijnen, M. H. Vasconcelos, I. J. Vechetti Jr., T. D. Veit, L. J. Vella, E. Velot, F. J. Verweij, B. Vestad, J. L. Vinas, T. Visnovitz, K. V. Vukman, J. Wahlgren, D. C. Watson, M. H. Wauben, A. Weaver, J. P. Webber, V. Weber, A. M. Wehman, D. J. Weiss, J. A. Welsh, S. Wendt, A. M. Wheelock, Z. Wiener, L. Witte, J. Wolfram, A. Xagorari, P. Xander, J. Xu, X. Yan, M. Yanez-Mo, H. Yin, Y. Yuana, V. Zappulli, J. Zarubova, V. Zekas, J. Y. Zhang, Z. Zhao, L. Zheng, A. R. Zheutlin, A. M. Zickler, P. Zimmermann, A. M. Zivkovic, D. Zocco and E. K. Zuba-Surma, *J. Extracell. Vesicles*, 2018, **7**(1), 1535750, DOI: 10.1080/20013078.2018.1535750.

3 A. Giovanazzi, M. J. C. van Herwijnen, M. Kleinjan, G. N. van der Meulen and M. H. M. Wauben, *Sci. Rep.*, 2023, **13**(1), 8758, DOI: 10.1038/s41598-023-35799-w.

4 J. Muller Bark, L. Trevisan Franca de Lima, X. Zhang, D. Broszczak, P. J. Leo, R. L. Jeffree, B. Chua, B. W. Day and C. Punyadeera, *Cancer*, 2023, **15**(129), 2836–2847, DOI: 10.1002/cncr.34888.

5 P. D. Stahl and G. Raposo, *Essays Biochem.*, 2018, **62**(2), 119–124, DOI: 10.1042/EBC20170088.

6 I. Nazarenko, S. Rana, A. Baumann, J. McAlear, A. Hellwig, M. Trendelenburg, G. Lochnit, K. T. Preissner and M. Zoller, *Cancer Res.*, 2010, **70**(4), 1668–1678, DOI: 10.1158/0008-5472.CAN-09-2470.

7 G. Raposo and W. Stoorvogel, *J. Cell Biol.*, 2013, **200**(4), 373–383, DOI: 10.1083/jcb.201211138.

8 T. P. Raposo, B. C. Beirao, L. Y. Pang, F. L. Queiroga and D. J. Argyle, *Vet. J.*, 2015, **205**(2), 161–174, DOI: 10.1016/j.tvjl.2015.04.015.

9 P. D. Stahl and G. Raposo, *Physiology*, 2019, **34**(3), 169–177, DOI: 10.1152/physiol.00045.2018.

10 E. I. Buzas, *Nat. Rev. Immunol.*, 2023, **23**(4), 236–250, DOI: 10.1038/s41577-022-00763-8.

11 Y. Couch, E. I. Buzas, D. Di Vizio, Y. S. Gho, P. Harrison, A. F. Hill, J. Lotvall, G. Raposo, P. D. Stahl, C. Thery, K. W. Witwer and D. R. F. Carter, *J. Extracell. Vesicles*, 2021, **10**(14), e12144, DOI: 10.1002/jev2.12144.

12 C. P. O'Neill, K. E. Gilligan and R. M. Dwyer, *Cancers*, 2019, **11**(2), 136, DOI: 10.3390/cancers11020136.

13 L. M. Doyle and M. Z. Wang, *Cells*, 2019, **8**(7), DOI: 10.3390/cells8070727.

14 J. P. Santavanond, S. F. Rutter, G. K. Atkin-Smith and I. K. H. Poon, *Subcell. Biochem.*, 2021, **97**, 61–88, DOI: 10.1007/978-3-030-67171-6_4.

15 M. Nawaz, G. Camussi, H. Valadi, I. Nazarenko, K. Ekstrom, X. Wang, S. Principe, N. Shah, N. M. Ashraf, F. Fatima, L. Neder and T. Kislinger, *Nat. Rev. Urol.*, 2014, **11**(12), 688–701, DOI: 10.1038/nrurol.2014.301.

16 M. Nawaz, F. Fatima, I. Nazarenko, K. Ekstrom, I. Murtaza, M. Anees, A. Sultan, L. Neder, G. Camussi, H. Valadi, J. A. Squire and T. Kislinger, *Expert Rev. Proteomics*, 2016, **13**(4), 395–409, DOI: 10.1586/14789450.2016.1165613.

17 J. B. Simonsen, *J. Extracell. Vesicles*, 2019, **8**(1), 1582237, DOI: 10.1080/20013078.2019.1582237.

18 A. Clayton, E. Boilard, E. I. Buzas, L. Cheng, J. M. Falcon-Perez, C. Gardiner, D. Gustafson, A. Gualerzi, A. Hendrix, A. Hoffman, J. Jones, C. Lasser, C. Lawson, M. Lenassi, I. Nazarenko, L. O'Driscoll, R. Pink, P. R. Siljander, C. Soekmadji, M. Wauben, J. A. Welsh, K. Witwer, L. Zheng and R. Nieuwland, *J. Extracell. Vesicles*, 2019, **8**(1), 1647027, DOI: 10.1080/20013078.2019.1647027.

19 C. L. Arteaga, M. X. Sliwkowski, C. K. Osborne, E. A. Perez, F. Puglisi and L. Gianni, *Nat. Rev. Clin. Oncol.*, 2011, **9**(1), 16–32, DOI: 10.1038/nrclinonc.2011.177.

20 C. Jackson, D. Browell, H. Gautrey and A. Tyson-Capper, *Int. J. Cell Biol.*, 2013, **2013**, 973584, DOI: 10.1155/2013/973584.

21 R. Saddawi-Konefka, S. Schokrpur, A. J. Lui and J. S. Gutkind, *Cancer J.*, 2022, **28**(5), 339–345, DOI: 10.1097/PPO.0000000000000622.

22 N. Dempsey, A. Sandoval and R. Mahtani, *Curr. Treat. Options Oncol.*, 2023, DOI: 10.1007/s11864-023-01108-w.

23 V. Ciravolo, V. Huber, G. C. Ghedini, E. Venturelli, F. Bianchi, M. Campiglio, D. Morelli, A. Villa, P. Della Mina, S. Menard, P. Filipazzi, L. Rivoltini, E. Tagliabue and S. M.

Pupa, *J. Cell. Physiol.*, 2012, **227**(2), 658–667, DOI: 10.1002/jcp.22773.
24 S. Liebhardt, N. Ditsch, R. Nieuwland, A. Rank, U. Jeschke, F. Von Koch, K. Friese and B. Toth, *Anticancer Res.*, 2010, **30**(5), 1707–1712.
25 A. Nanou, L. L. Zeune, F. C. Bidard, J. Y. Pierga and L. Terstappen, *Breast Cancer Res.*, 2020, **22**(1), 86, DOI: 10.1186/s13058-020-01323-5.
26 J. Wang, H. Xie and C. Ding, *ACS Appl. Mater. Interfaces*, 2021, **13**(28), 32837–32844, DOI: 10.1021/acsami.1c09388.
27 W. Chen, Z. Li, W. Cheng, T. Wu, J. Li, X. Li, L. Liu, H. Bai, S. Ding, X. Li and X. Yu, *J. Nanobiotechnol.*, 2021, **19**(1), 450, DOI: 10.1186/s12951-021-01210-x.
28 U. Bog, F. Brinkmann, H. Kalt, C. Koos, T. Mappes, M. Hirtz, H. Fuchs and S. Kober, *Small*, 2014, **10**(19), 3863–3868, DOI: 10.1002/smll.201400813.
29 S. F. Wondimu, M. Hippler, C. Hussal, A. Hofmann, S. Krammer, J. Lahann, H. Kalt, W. Freude and C. Koos, *Opt. Express*, 2018, **26**(3), 3161–3173, DOI: 10.1364/OE.26.003161.
30 S. F. Wondimu, S. von der Ecken, R. Ahrens, W. Freude, A. E. Guber and C. Koos, *Lab Chip*, 2017, **17**(10), 1740–1748, DOI: 10.1039/c6lc01556e.
31 O. Scheler, J. T. Kindt, A. J. Qavi, L. Kaplinski, B. Glynn, T. Barry, A. Kurg and R. C. Bailey, *Biosens. Bioelectron.*, 2012, **36**(1), 56–61, DOI: 10.1016/j.bios.2012.03.037.
32 Z. Feng and L. Bai, *Micromachines*, 2018, **9**(3), DOI: 10.3390/mi9030122.
33 T. Wienhold, S. Kraemmer, S. F. Wondimu, T. Siegle, U. Bog, U. Weinzierl, S. Schmidt, H. Becker, H. Kalt, T. Mappes, S. Koeber and C. Koos, *Lab Chip*, 2015, **15**(18), 3800–3806, DOI: 10.1039/c5lc00670h.
34 J. Kowal, G. Arras, M. Colombo, M. Jouve, J. P. Morath, B. Primdal-Bengtson, F. Dingli, D. Loew, M. Tkach and C. Thery, *Proc. Natl. Acad. Sci. U. S. A.*, 2016, **113**(8), E968–E977, DOI: 10.1073/pnas.1521230113.
35 J. Codony-Servat, J. Albanell, J. C. Lopez-Talavera, J. Arribas and J. Baselga, *Cancer Res.*, 1999, **59**(6), 1196–1201.
36 H. Im, H. Shao, Y. I. Park, V. M. Peterson, C. M. Castro, R. Weissleder and H. Lee, *Nat. Biotechnol.*, 2014, **32**(5), 490–495, DOI: 10.1038/nbt.2886.
37 I. M. White and X. Fan, *Opt. Express*, 2008, **16**(2), 1020–1028, DOI: 10.1364/oe.16.001020.
38 K. Boriachek, M. N. Islam, A. Moller, C. Salomon, N. T. Nguyen, M. S. A. Hossain, Y. Yamauchi and M. J. A. Shiddiky, *Small*, 2018, **14**(6), DOI: 10.1002/smll.201702153.
39 K. Singh, R. Nalabotala, K. M. Koo, S. Bose, R. Nayak and M. J. A. Shiddiky, *Analyst*, 2021, **146**(12), 3731–3749, DOI: 10.1039/d1an00024a.
40 T. Akagi, K. Kato, M. Kobayashi, N. Kosaka, T. Ochiya and T. Ichiki, *PLoS One*, 2015, **10**(4), e0123603, DOI: 10.1371/journal.pone.0123603.
41 S. Lee, B. P. Crulhas, S. Suvakov, S. V. Verkhoturov, D. S. Verkhoturov, M. J. Eller, H. Malhi, V. D. Garovic, E. A. Schweikert, G. Stybayeva and A. Revzin, *ACS Appl. Mater. Interfaces*, 2021, **13**(44), 52321–52332, DOI: 10.1021/acsami.1c14506.
42 B. Martin-Gracia, A. Martin-Barreiro, C. Cuestas-Ayllon, V. Grazu, A. Line, A. Llorente, J. M. de la Fuente and M. Moros, *J. Mater. Chem. B*, 2020, **8**(31), 6710–6738, DOI: 10.1039/d0tb00861c.
43 M. Gaillard, A. Thuaire, G. Nonglaton, V. Agache, Y. Roupioz and C. Raillon, *Analyst*, 2020, **145**(6), 1997–2013, DOI: 10.1039/c9an01949a.
44 P. Todeschini, E. Cocco, S. Bellone, J. Varughese, K. Lin, L. Carrara, F. Guzzo, N. Buza, P. Hui, D. A. Silasi, E. Ratner, M. Azodi, P. E. Schwartz, T. J. Rutherford, S. Pecorelli and A. D. Santin, *Br. J. Cancer*, 2011, **105**(8), 1176–1182, DOI: 10.1038/bjc.2011.369.
45 A. Perrier, J. Gligorov, G. Lefevre and M. Boissan, *Lab. Invest.*, 2018, **98**(6), 696–707, DOI: 10.1038/s41374-018-0033-8.
46 S. Eppenberger-Castori, D. Klingbiel, T. Ruhstaller, D. Dietrich, D. A. Rufle, K. Rothgiesser, O. Pagani and B. Thurlimann, *BMC Cancer*, 2020, **20**(1), 114, DOI: 10.1186/s12885-020-6594-0.
47 C. Gardiner, M. Shaw, P. Hole, J. Smith, D. Tannetta, C. W. Redman and I. L. Sargent, *J. Extracell. Vesicles*, 2014, **3**, 25361, DOI: 10.3402/jev.v3.25361.
48 A. Takeda, A. Tachibana, H. Nagumo and K. Sakai-Kato, *Anal. Biochem.*, 2023, **669**, 115130, DOI: 10.1016/j.ab.2023.115130.
49 D. Bachurski, M. Schuldner, P. H. Nguyen, A. Malz, K. S. Reiners, P. C. Grenzi, F. Babatz, A. C. Schauss, H. P. Hansen, M. Hallek and E. Pogge von Strandmann, *J. Extracell. Vesicles*, 2019, **8**(1), 1596016, DOI: 10.1080/20013078.2019.1596016.
50 B. Bettin, A. Gasecka, B. Li, B. Dhondt, A. Hendrix, R. Nieuwland and E. van der Pol, *J. Thromb. Haemostasis*, 2022, **20**(11), 2679–2685, DOI: 10.1111/jth.15867.
51 R. Nieuwland and P. R. Siljander, *J. Extracell. Vesicles*, 2024, **13**(1), e12400, DOI: 10.1002/jev2.12400.
52 J. Nouvel, G. B. Quevedo, T. Prinz, R. Masood, G. Daaboul, T. Gainey-Schleicher, U. Wittel, S. Chikhladze, B. Melykuti, M. Helmstaedter, K. Winkler, I. Nazarenko and G. Putz, *J. Extracell. Vesicles*, 2024, **13**(10), e70008, DOI: 10.1002/jev2.70008.
53 J. A. Welsh, D. C. I. Goberdhan, L. O'Driscoll, E. I. Buzas, C. Blenkiron, B. Bussolati, H. Cai, D. Di Vizio, T. A. P. Driedonks, U. Erdbrugger, J. M. Falcon-Perez, Q. L. Fu, A. F. Hill, M. Lenassi, S. K. Lim, M. G. Mahoney, S. Mohanty, A. Moller, R. Nieuwland, T. Ochiya, S. Sahoo, A. C. Torrecilhas, L. Zheng, A. Zijlstra, S. Abuelreich, R. Bagabas, P. Bergese, E. M. Bridges, M. Brucale, D. Burger, R. P. Carney, E. Cocucci, R. Crescitelli, E. Hanser, A. L. Harris, N. J. Haughey, A. Hendrix, A. R. Ivanov, T. Jovanovic-Talisman, N. A. Kruh-Garcia, V. Ku'ulei-Lyn Faustino, D. Kyburz, C. Lasser, K. M. Lennon, J. Lotvall, A. L. Maddox, E. S. Martens-Uzunova, R. R. Mizenko, L. A.

Newman, A. Ridolfi, E. Rohde, T. Rojalin, A. Rowland, A. Saftics, U. S. Sandau, J. A. Saugstad, F. Shekari, S. Swift, D. Ter-Ovanesyan, J. P. Tosar, Z. Useckaite, F. Valle, Z. Varga, E. van der Pol, M. J. C. van Herwijnen, M. H. M. Wauben, A. M. Wehman, S. Williams, A. Zendrini, A. J. Zimmerman, M. Consortium, C. Thery and K. W. Witwer, *J. Extracell. Vesicles*, 2024, **13**(2), e12404, DOI: 10.1002/jev2.12404.

54 J. Lahann, I. S. Choi, J. Lee, K. F. Jensen and R. Langer, *Angew. Chem., Int. Ed.*, 2001, **40**(17), 3166–3169, DOI: 10.1002/1521-3773(20010903)40:17<3166::AID-ANIE3166>3.0.CO;2-#.